

Document downloaded from:

<http://hdl.handle.net/10251/141648>

This paper must be cited as:

González-Guisasola, C.; Ribes-Greus, A. (05-2). Dielectric Relaxations and Conductivity of Crosslinked PVA/SSA/GO Composite Membranes for Fuel Cells. *Polymer Testing*. 67:55-67. <https://doi.org/10.1016/j.polymertesting.2018.01.024>



The final publication is available at

<https://doi.org/10.1016/j.polymertesting.2018.01.024>

Copyright Elsevier

Additional Information

Dielectric Relaxations and Conductivity of Cross-linked PVA/SSA/GO Composite Membranes for Fuel Cells

C.González-Guisasola¹, A. Ribes-Greus^{1,*}

This is an open-access version, according to <http://www.sherpa.ac.uk/romeo/issn/0142-9418/>

Full text available at: <https://www.sciencedirect.com/science/article/pii/S0142941817317026>

DOI: <https://doi.org/10.1016/j.polymertesting.2018.01.024>

Please, cite it as:

C.González-Guisasola, A. Ribes-Greus. Dielectric Relaxations and Conductivity of Cross-linked PVA/SSA/GO Composite Membranes for Fuel Cells. Polymer testing 2018;67:55-67

¹Instituto de Tecnología de Materiales (ITM).
Universitat Politècnica de València.
Camino de Vera s/n, 46022 Valencia, Spain.

*Corresponding author:

A. Ribes-Greus
aribes@ter.upv.es
Tel. 0034 630125695

Dielectric Relaxations and Conductivity of Cross-linked PVA/SSA/GO Composite Membranes for Fuel Cells

C.González-Guisasola¹, A. Ribes-Greus^{1,*}.

Abstract

Composite membranes obtained from Poly(vinyl Alcohol) (PVA) with sulfosuccinic acid (SSA) as crosslinking agent, and two different proportions of graphene oxide (GO), were prepared to be used in Proton Exchange Membrane Fuel Cells (PEMFCs). The superficial micrographs from transmission electron microscopy (TEM) confirmed a good dispersion of GO. Fourier Transform Infrared spectroscopy (FTIR) was used to evaluate the final chemical structure. Differential Scanning Calorimetry (DSC) showed that glass transition and crystalline phase were not present in the cross-linked PVA/SSA/GO composites membranes. Thermogravimetric analysis (TGA) demonstrated that the addition of GO reduced the moisture content and increased the thermal stability of the membranes. The electrical properties of PVA/SSA and PVA/SSA/GO composite membranes and the effect of GO concentration were evaluated by means of dielectric spectra in a broad range of temperatures and frequencies. The dielectric permittivity of these membranes was significantly promoted at low filler concentration due to an interfacial polarization effect. From the analysis of the dielectric relaxation spectrum, it can be deduced that the origin of the associated molecular movements is intramolecular and occurs in the working range of the PEMFC. In addition, the direct current conductivity, the protonic conductivity, and the polarization currents were correlated to the power produced in a hydrogen monocell. It was observed that low and no high GO concentrations of filler in PVA/SSA composite membranes enhanced their performance. The systematic characterization procedure based on the study of dielectric spectra and conductivity allowed to establish a potential approach to control the addition of GO in the design of other composite membranes for PEMFC with improved properties.

Keywords

Poly(vinyl alcohol); Nanocomposite membrane; Graphene oxide (GO); Dielectric relaxation spectra; Protonic conductivity; Proton Exchange Membranes Fuel Cell (PEMFC)

1. Introduction

Polymer electrolyte membranes of low-temperature fuel cells (PEMFC) have attracted increasing attention because they are considered as a clean and ecological energy solution to the global rising power demand [1]. It is recognised that an efficient PEMFC depends, among other factors, on the polymer electrolyte membranes (PEM). This kind of membranes requires very specific conditions such as good mechanical, dimensional and chemical stability in an environment of high humidity. Nafion® (Dupont) is by far one of the best performing low-temperature polymer electrolyte membranes. However, one of the drawbacks of these membranes is their relatively high cost [2], [3]. One alternative to overcome this disadvantage is the preparation of composite membranes from Poly(vinyl Alcohol (PVA) and graphene oxide (GO), a low cost eco-friendly polymer.

PVA is a hydrophilic, semicrystalline polymer with a structure consisting of a carbon chain backbone with hydroxyl (-OH) groups attached laterally. However, PVA membranes are poor proton conductors compared to Nafion® membranes because PVA itself has not enough negatively charged ions such as carboxylic and sulfonic acid groups. Therefore, PVA as membrane electrolyte is usually cross-linked by a transesterification process with sulfosuccinic acid (SSA) [4] to improve the mechanical properties and increase the sulfonic group content in the polymer matrix [5], [6]. Nevertheless, the cross-linked PVA/SSA composites membranes performance in a fuel cell device does not reach the same behaviour than a commercial membrane of Nafion®.

Extensive studies aimed to increase the properties of PVA/SSA composites membranes with either ionic [5], [7]–[13] or non-ionic [14], [15] fillers. The small amounts of filler are able to produce a remarkable increase of specific surface area, leading to enhanced interfacial interactions at the interface between matrix and filler. The addition of inorganic nano-sized fillers from semimetal oxides allows the improvement of the thermal and chemical resistance [16], [17] but also increases the fragility associated to the percentage of load [18]. Among the many types of filler, GO is a good candidate because its functionality is derived from sp² and sp³ carbon [18]–[22], which improves the filler matrix compatibility and offers interesting permittivity enhancements without adversely affecting the dielectric losses. The presence of functional groups at the surface is a source of hydrogen bonding which is expected to collaborate in the protonic conductivity by transfer and proton-giving in films for PEMFC [23], [24]. Thus, the interfacial interaction between filler and PVA matrix plays an important role and regulates the dielectric properties. Despite the dielectric properties increase with the amount of filler, this is limited due to the tendency of the filler to form bundled agglomerates in the polymer matrix.

Impedance analysis and polarization currents are sensitive techniques to study the dielectric behaviour of polymers. It can reveal the microstructural details of the materials at molecular and macroscopic levels. The dielectric constant and dissipation factor are crucial properties to design suitable polymer electrolyte membranes, and to allow the understanding of the polarizing mechanism and the conductivity [25]–[28]. Despite electrical properties of pure and filled PVA films have been studied by many authors [29]–[35], previous works were focused on analysing the evolution of electrical properties and the molecular dynamics of PVA/SSA/GO composites membranes when the proportion of GO increases.

The aim of the current study is to correlate the dielectric properties, molecular dynamics, and conductivity with the composition of the membrane to predict its behaviour. For that reason, a systematic characterization of the chemical structure and morphology of several PVA/SSA/GO composite membranes was carried out. Properties as polarization, dielectric permittivity,

electronic and protonic conductivity were determined and connected to the filler composition of GO in the membrane. The dielectric relaxation spectrum was studied and the inter or intramolecular origin of these relaxation processes, as an Arrhenius or Vogel-Tamman-Fulcher behaviour, was discussed and related to the Grotthuss or proton hopping mechanism because the proton conductivity depends on the molecular mobility. It was observed that low GO concentrations of filler enhanced the performance of these membranes and provided a potential strategy based on graphene oxide, which would improve the performance of these and other composite membranes in PEMFC.

2. Experimental

2.1 Materials and preparation of composites membranes

Graphene oxide was prepared from graphite powder using the Modified Hummers Method (MHM) [36],[37]. Briefly, graphite powder (<20 μ m) was mixed with H₂SO₄ and NaNO₃, and refrigerated in an ice bath to maintain the temperature below 20 °C. Then, KMnO₄ was added gradually to the solution under constant stirring. Afterwards, the mixture was diluted in distilled water and the temperature was raised to 98 °C. To reduce the remaining KMnO₄, a H₂O₂ solution 30% was added and the solid phase was washed several times with HCl 37% and EtOH until neutral pH was reached. Finally, the GO powder was filtered and dried in a vacuum oven at 60 °C.

A series of nanocomposite films of PVA/SSA and PVA/SSA/GO composite membranes PVA/SSA/GO were prepared following a previously described procedure [38]. PVA substrates with hydrolysis degrees of 86.7–88.9% and molecular weight-average of 67000 g·mol⁻¹ were solved in distilled water, mixed with GO powder, refluxed at 90°C and subsequently cooled down to room temperature. Then, a 30% SSA in distilled water solution was gradually added to the PVA solution with continuous agitation for 24 hours. Finally, the resulting solution was cast on a Teflon® mould dish and it was cross-linked at 110 °C during 2 hours. The thickness of the membranes was about 120 μ m. The membranes were labelled as PVA/SSA, PVA/SSA/GO-0.5 and PVA/SSA/GO-1.0 to indicate whether the membrane had no GO or its proportion loading was 0.5 and 1 wt%, respectively.

A membrane of Nafion® was used as reference membrane. This membrane was pre-treated by immersing the membrane in three consecutive baths of 3% H₂O₂, 0,5M H₂SO₄ and distilled water [39].

2.2 Characterisation techniques

The Transmission Electron Microscopy (TEM) images were obtained to observe the microstructure and dispersion of GO nanoparticles in PVA/SSA/GO composite membranes, by using a JEM 1010 electron microscope (JEOL, Japan) at an accelerating voltage of 100 kV.

Fourier Transform Infrared spectroscopy (FTIR) experiments to analyse the final chemical structure of PVA/SSA/GO composite membranes were performed using a Thermo Nicolet 5700 Fourier transform infrared spectrometer with an attenuated total reflectance accessory (ATR).

Differential Scanning Calorimetry (DSC), thermograms were obtained using a Mettler Toledo DSC 822 analyser. Samples of around 5 mg were heated up from 25 °C to 220 °C at 10 °C·min⁻¹.

All experiments were run under nitrogen atmosphere ($50 \text{ ml}\cdot\text{min}^{-1}$). Three consecutive scans of heating, cooling and heating were carried out.

Moisture content and stability of the membranes were determined by Thermogravimetric Analysis (TGA) by means of a Mettler-Toledo TGA 851 analyser. The samples, with a mass of about 4 mg were introduced in an alumina holder, with capacity of $70 \mu\text{l}$. The samples were analysed in the temperature range of 25 to $800 \text{ }^\circ\text{C}$ at different heating rate of $10^\circ\text{C}\cdot\text{min}^{-1}$, under atmosphere of oxygen at a flow rate of $50 \text{ ml}\cdot\text{min}^{-1}$. The moisture content was evaluated by the decrease of loss mass and the peak temperature (T_p) from the first-differential TG curve, i.e. the DTG curve, related to the inflection temperature of the TG curve, was also considered.

The dielectric spectrum of each sample was recorded by a Concept 40 high performance dielectric spectrometer (Novocontrol GmbH). To assure stability in the measurements, all experiments were exposed to a heated gas stream coming from evaporating liquid nitrogen in a Dewar flask. Temperature control was performed by a Novocontrol Quatro cryo-system ($\pm 0.1 \text{ }^\circ\text{C}$), at the frequency range between 10^{-2} to 10^7 Hz and starting at $-150 \text{ }^\circ\text{C}$ and raised in $10 \text{ }^\circ\text{C}$ increments up to $100 \text{ }^\circ\text{C}$. This temperature was considered because it may be a limit value for a low temperature fuel cell. To carry out these dielectric experiments, Teflon® guard were placed between the stainless steel electrodes (SSE), to avoid the masking effect of the conductivity contribution in the low frequency range. The dielectric response is measured in terms of loss tangent δ , real ϵ' and imaginary ϵ'' permittivity which represent the storage and loss of energy in each cycle of the applied electric field.

Protonic conductivity was performed at the frequency range between 10^{-2} to 10^7 Hz at room temperature. The Teflon® guard was avoided between stainless steel electrodes (SSE). The PVA/SSA/GO composite membranes were previously hydrated during 24 h.

The measurements for the polarization experiments were registered using a Keithley model 6420 electrometer and a lab-made controlled contact cell. The samples were hold between two stainless steel electrodes (SSE) of 20 mm diameter, forming a parallel plate capacitor. The sample cell was mounted inside a controlled temperature furnace. The total ionic transfer number and conductivity were then determined.

The fuel cell performance test consisted in an H-Tec fuel cell kit, a lab-made decade resistor, a Keithley 2410 and a Fluke 73 DMM. Reactant gasses were produced in situ by water electrolysis and collected in hydrostatic sealed deposits. The composite membranes were hydrated and placed between two 4 cm^2 carbon cloths ($2 \text{ mg}\cdot\text{cm}^{-2}$ Pt black, FuelCellsEtc). The measurements were performed at room temperature and taken when a stable current value was reached.

3. Results and discussion

3.1 Surface morphology

The microstructure of PVA/SSA and all PVA/SSA/GO composite membranes is displayed in **Figure 1**. As expected, PVA/SSA composite membrane presented a uniform structure without nanoparticles **Figure 1a**. On the other hand, PVA/SSA/GO-0.5 composite membranes showed good nanoparticle dispersion **Figure 1b**.



Figure 1. TEM images for (a) PVA/SSA, (b) PVA/SSA/GO-0.5, and (c) PVA/SSA/GO-1.0.

In contrast, PVA/SSA/GO-1 composite membranes showed randomly dispersed dark inclusions, suggesting that GO formed agglomerates **Figure 1c**. It is known that GO presents hydroxyl groups in its basal plane and carboxylic and ketone groups in the edges, as can be seen in **Figure 2**. These charged groups could induce the coagulation of particles during the preparation process in the samples with higher concentration of GO [18], [40]–[42]

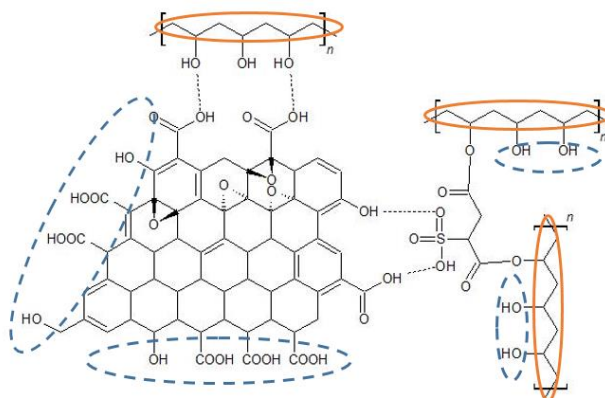


Figure 2. Some possible GO supramolecular interactions in cross-linked PVA/SSA/GO membranes.

3.2 Structural characterization

FTIR spectroscopy is a very useful technique for analyzing polymer structures. **Figure 3** shows the respective infrared spectra for PVA, SSA, GO and PVA/SSA/GO PVA composite membranes. The different regions of the FT-IR spectra of the PVA are plotted in **Figure 3a**. It contains distinct contributions arising from the structural components of the PVA homopolymer including: the OH stretching region associated to the alcohol groups; the asymmetric and symmetric stretching vibrations of the CH₂ groups; the vibration bands of scissoring in CH₂; the vibration stretching of the acetyl and alcohol groups. **Figure 3b** displays the FTIR spectrum of SSA, a broadband linked to the carboxylic acid groups, the sulfonic group and the water molecules, which overlaps the characteristic ester absorption band. In **Figure 3c** appears the characteristic peaks of FTIR spectrum of GO attributed to stretching vibration bands of the –OH/H₂O, carboxylic group and epoxy groups which confirms the existence of the oxidized forms of graphene. **Table 1** summarized the assignments of these absorption bands.

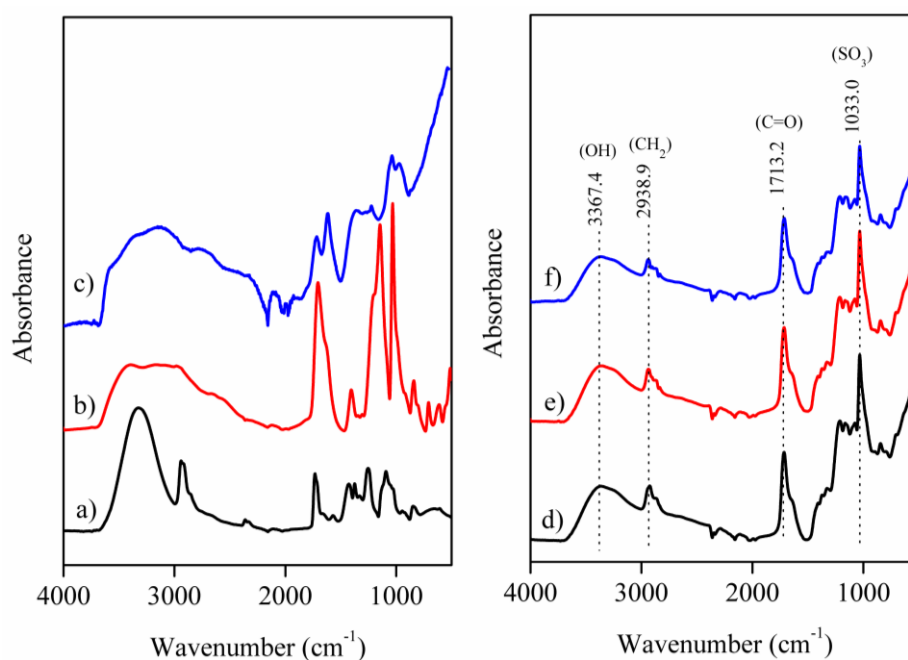


Figure 3. FT-IR spectra of a) PVA, b) SSA, c) GO, d) PVA/SSA/GO-0, e) PVA/SSA/GO-0.5 and f) PVA/SSA/GO-1.0 series polymers.

The FTIR spectra of PVA/SSA/GO composite membranes with 0, 0.5 and 1% of GO composition are depicted in **Figure 3d**, **3e** and **3f** respectively. These spectra reflect characteristic FTIR peaks of each component present in the composite. The intensity of the peaks is reduced when compared to the FTIR spectrum of pure polymers. **Table 1** summarized the assignments of these absorption bands. The maximum value of the absorbance corresponding to OH, CO, COC and SO₃ groups was normalized to the band of the CH₂ groups ($\nu \sim 2940 \text{ cm}^{-1}$) [43]. The positions and relative intensities for the main peaks in PVA, SSA, GO, PVA/SSA and its PVA/SSA/GO composite membranes can be found in **Table 2**.

Table 1. Main infrared absorption bands for PVA, SSA, GO and PVA composites.

Wavenumber (cm ⁻¹)	Assignment	Contribution	Reference
3600-3000	OH stretching	PVA, SSA, H ₂ O	[4], [6], [43]–[48]
2910-2950	Asymmetric/symmetric CH ₂ stretching	PVA, SSA	[4], [45], [49]
1790-1660	CO stretching	Acetate groups PVA, carboxyl groups SSA	[4], [18], [43], [45], [46], [48], [50]
1615	C=C	Aromatic bond from GO	[51]–[53]
1426	CH ₂ stretching	PVA	[4]
1374	CH bending	PVA	[4], [18], [43], [45], [46], [48], [50]
1220-1253	CO stretching	Residual acetate from non-hydrolyzed PVA, GO	[4], [18], [43]
1092	COH stretching	PVA	
1033	SO ₃ and epoxy stretching	SO ₃ from SSA, epoxy from GO	[4], [51], [54]–[59]

The evaluation of the FTIR response of the PVA/SSA and PVA/SSA/GO composite membranes was studied in more detail to analyze the intermolecular interactions between the functional groups. The crosslinking with SSA causes a shift to lower wavenumbers and a reduction in the intensity of the OH band (I_{OH}) of the composites due to the reaction of the hydroxyl groups of the host polymer and the carboxylic groups of the SSA unit [38], [54], [60]–[62]. An increase of the interfacial hydrogen interactions by the GO addition [63] was also observed. The intensity of the SO_3 band increases with the addition of the sulfonic group to the polymer, confirming a successful crosslinking since SSA contains $-SO_3H$ groups [4], [38], [51], [54]–[59]. Additionally, there is an increase in the absorbance values of the CO and COC bands (I_{CO} and I_{COC} , respectively) due to the creation of new ester bonds [38], [48]. These bands also move to lower wavenumbers in the membranes with GO, indicating an increase in the hydrogen bonding which can enhance the protonic conductivity of these membranes.

Table 2. Position and relative intensities of characteristic bands for PVA and its PVA/SSA/GO composite membranes.

Sample	OH st		CO st	
	ν_{max} (cm^{-1})	I_{OH}	ν_{max} (cm^{-1})	I_{CO}
PVA	3591.24	1.76	1732.5	0.82
PVA/SSA	3366.7	1.00	1714.4	1.64
PVA/SSA/GO-0.5	3364.4	1.07	1714.3	1.83
PVA/SSA/GO-1.0	3367.4	1.07	1713.2	2.01
Sample	COC st		SO_3 st	
	ν_{max} (cm^{-1})	I_{COC}	ν_{max} (cm^{-1})	I_{SO_3}
PVA	1253.5	0.89	-----	-----
PVA/SSA	1211.4	2.24	1032.9	3.50
PVA/SSA/GO-0.5	1212.1	2.44	1033.1	3.76
PVA/SSA/GO-1.0	1211.5	2.55	1033.2	3.78

3.3 Thermal properties

Differential scanning calorimetry (DSC) is relevant to determine the crystallinity degree and the static glass transition of cross-linked membranes. The thermograms corresponding to the first heating, cooling, and second heating, of the PVA/SSA and PVA/SSA/GO composite membranes are shown in **Figure 4**. The first and the second heating thermograms are completely different because, in the first one, the most relevant phenomenon is the elimination of water, which probably occurs through two transitions related to the amount of free or link water occluded in the polymer matrix. The addition of GO induce a decrease of the peaks because less water is present in the matrix. The GO directly interact with OH groups, decreasing the number of PVA-water hydrogen bonds. Thus, the number of available OH hydration sites to attach water molecules decrease and consequently the moisture content. Since less amount of water is present in PVA/SSA/GO composite membranes, the evaporation of water region is less evident. In addition, the first cooling and second heating thermograms demonstrates that there is no glass transition and crystallinity, and it is consequently difficult to determine if this transition appears in the temperature range analysed. This fact confirms that the cross-linking of the chains together with the addition of GO reduces humidity and hinders both cooperative movements and the folding of the chains. Therefore, neither the glass transition nor the crystallization in the temperature range of operation of the PEMFC is present and the stability of the membranes might increase. To analyse the stability, a thermogravimetric analysis was carried out.

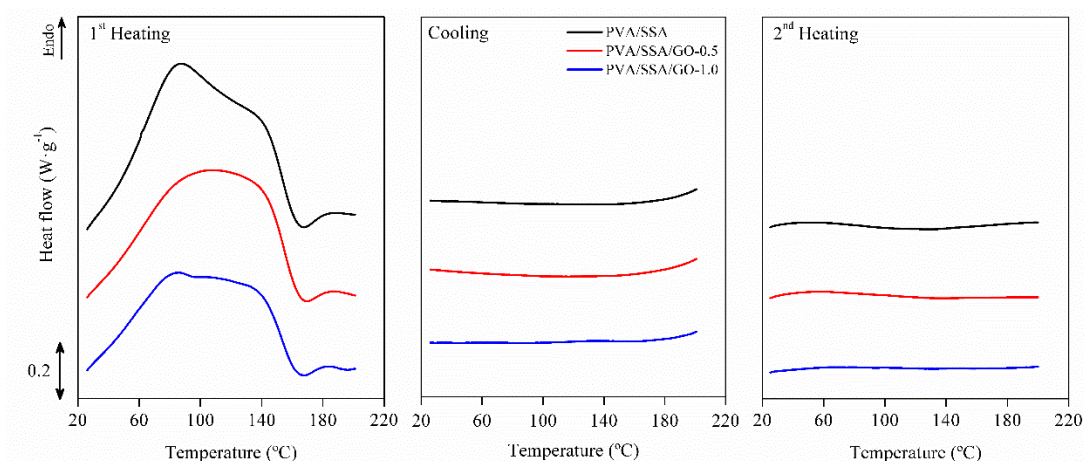


Figure 4. DSC for PVA/SSA (black), PVA/SSA/GO-0.5 (red) and PVA/SSA/GO-1 (blue).

Figure 5 shows thermogravimetric scan and the first-order thermograms of PVA/SSA and PVA/SSA/GO composite membranes. All the membranes exhibited three differentiated mass-loss stages, according to reported results for PVA-based materials [61], [64].

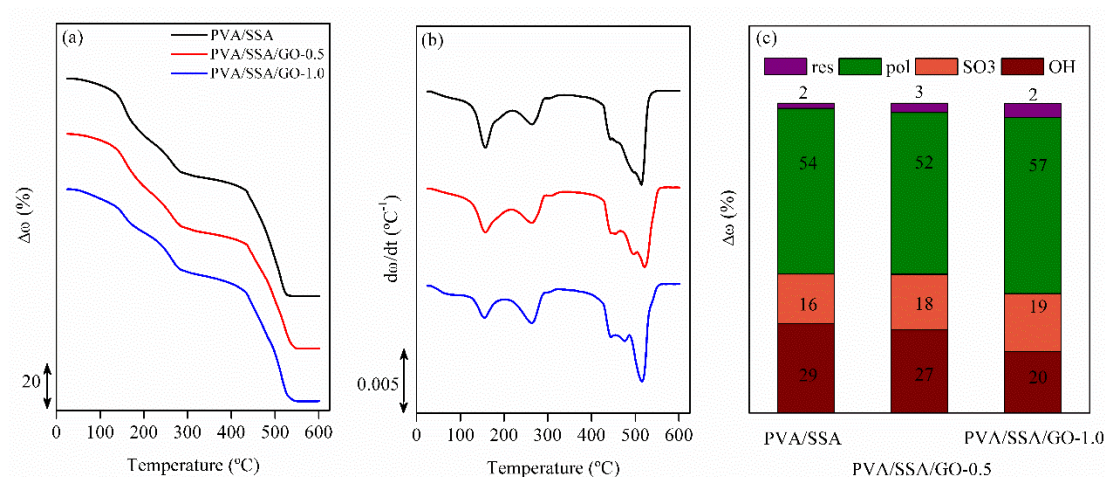


Figure 5. Thermogravimetric analysis and its corresponding derivative for PVA/SSA (black), PVA/SSA/GO-0.5 (red) and PVA/SSA/GO-1 (blue).

The first slight initial loss between 50 and 150 °C can be related to the remnant water present in the membranes followed by the decomposition of the hydroxyl groups. Then, the second stage near to 250 °C is attributed to the desulfonation process. The third decomposition stage is observed around 350 to 750 °C and corresponds to the breakdown of ether cross-linkages and main chain by means of chain-scission mechanism. The DTG curve shows more relevant temperature peaks. The moisture content for each membrane was evaluated by the decrease of loss mass calculated directly from the thermograms curves and is plotted in **Figure 5c**. The addition of GO reduces humidity and increases the thermal stability of the composites. The hydroxyl, carboxylic and carbonyl edges groups of GO increase the stabilization of the structure by means of the interfacial adhesion between the host matrix and the filler due to hydrogen bonding interactions.

3.4 Dielectric relaxations spectrum

PVA/SSA and PVA/SSA/GO composite membranes exhibit electrical relaxation phenomena, associated with the mobility of polar groups and interfacial interactions. The dielectric response provides valuable information with respect to polarization, dipole motions, and their mutual influence on the properties of the composite membranes. The dielectric response is generally described by the complex permittivity, ϵ^* , where real, ϵ' , and imaginary, ϵ'' , components represent the storage and loss of energy in each cycle of the applied electric field $\epsilon^* = \epsilon' - i \epsilon''$, and the loss tangent $\tan\delta = \epsilon''/\epsilon'$, as the relationship between both.

Figure 6 displays the dielectric response of PVA/SSA and PVA/SSA/GO composite membranes overviewed in the 3D plot showing the isothermal loss tangent curve in a broad range of frequency. These plots indicate that two individual processes are visible between -150 and 100 °C in all the samples, which are labelled as other authors as β and $\alpha\beta$ [65].

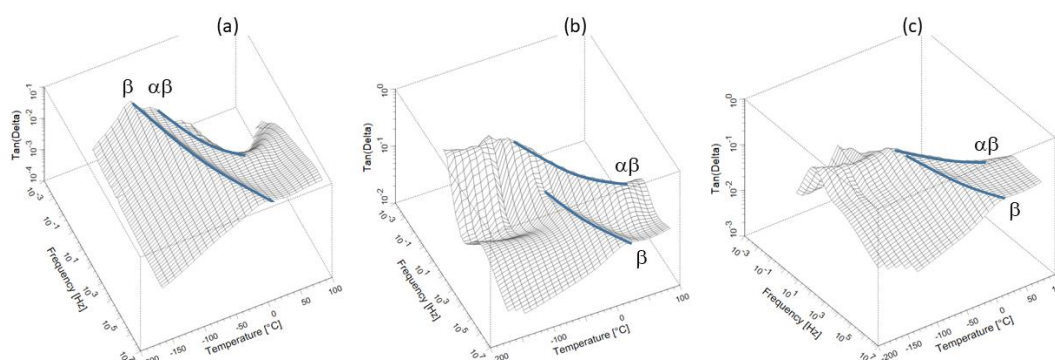


Figure 6. Frequency and temperature dependence of $\tan \delta$ for a) PVA/SSA, b) PVA/SSA/GO-0.5 and c) PVA/SSA/GO-1.0.

Figure 7 shows the corresponding 2D isochronal plots of PVA/SSA and PVA/SSA/GO composite membranes in terms of $\tan \delta$. As temperature increase, all samples exhibited a complexed relaxation zone that might be composed by a two-relaxation process, which molecular origin is controversial. The molecular movements of these relaxations might be probably associated to lateral groups, in this case, related to motions of hydroxyl groups, or movements of the main chain involving a small number of carbon atoms [66]. However, the moisture and GO content can have an important effect due to the evaporation transition and the bonding interaction between hydroxyl and carboxylic groups of GO with PVA/SSA host matrix, as can be seen in **Figure 2**.

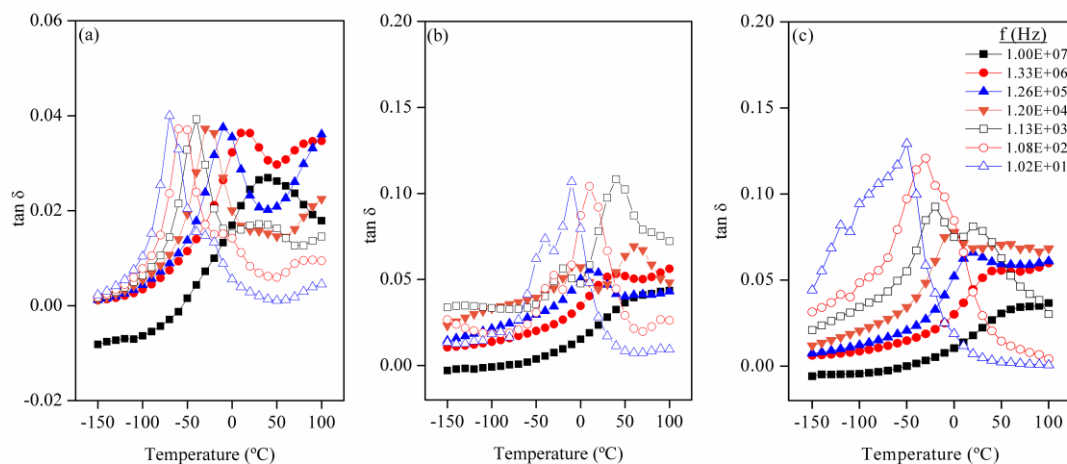


Figure 7. $\tan \delta$ for a) PVA/SSA, b) PVA/SSA/GO-0.5 and c) PVA/SSA/GO-1.0 with temperature.

Figure 8 shows the isothermal dielectric relaxation spectrum of PVA/SSA and PVA/SSA/GO composite membranes, in terms of the real part of the dielectric permittivity, at the frequency range from 10^{-2} to 10^7 Hz, and between -150 and 100 °C. It is clearly seen that ϵ' values were maximum at low frequency and high temperatures and remained ineffective because at lower frequencies the orientation of dipoles does not exist. However, due to molecular group's movements, the ϵ' values decreased with the temperature and higher frequencies. It was also found that the storage permittivity strongly increased by the addition of GO filler especially for the 0.5% percentage. However, for higher contents of filler, the ϵ' values decreased due to the formation of agglomerates, which in turns affects the improvement of the final properties.

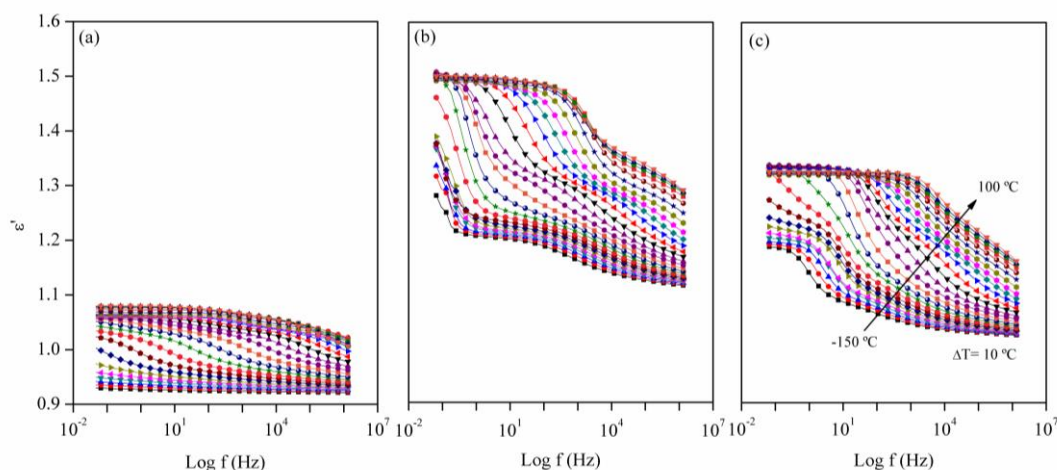


Figure 8. The real part of dielectric permittivity vs frequency of a) PVA/SSA, b) PVA/SSA/GO-0.5, c) PVA/SSA/GO-1.0.

Figure 9 and **10** display the β and $\alpha\beta$ relaxations in the isothermal and isochronal scans respectively in terms of the imaginary part of the dielectric permittivity.

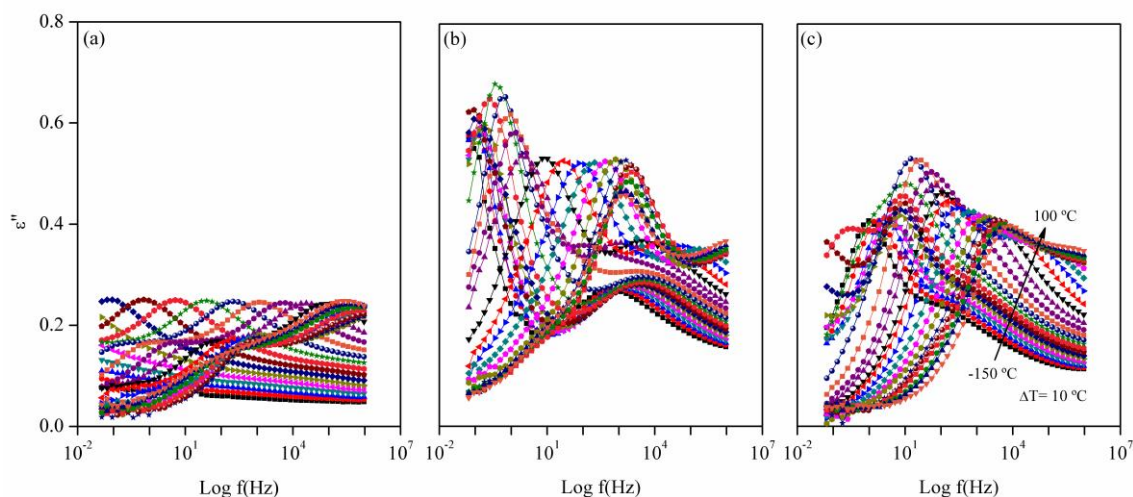


Figure 9. The imaginary part of dielectric permittivity for PVA/SSA (a), 0.5 wt% composite sample (b) and 1.0 wt% composite sample (c).

It can also be noticed that the temperature influences the dielectric loss modulus of the samples and the intensity of these relaxations raises when increases the temperature, especially at low frequencies [27]. The hydroxyl groups have also a strong influence on the PVA/SSA molecular dynamics due to the bonding interaction between OH neighbours and absorbed moisture. The elimination of free water, when the temperature increases, can represent a transition from different molecular mobility. However, the water-polymer motion is restricted by the presence of GO particles, which reduces moisture content. Both relaxations shifted to a higher temperature when GO content increased, as a result from both lower moisture content, as demonstrated by the calorimetric and thermogravimetric thermograms, and lower mobility, caused by the bonding interaction between the particles of GO and PVA/SSA matrix.

Another important issue is the molecular origin of the observed relaxation processes and discerning whether the molecular movement that produces one of these relaxations is associated with the glass transition or is typical from a secondary relaxation.

The ascription to a glass transition of one of these relaxations has led to misinterpretation [65]–[67] because the static glass transition is difficult to observe in the DSC calorimetric thermograms. Thus, in order to identify the molecular origin of relaxations and assess the influence of GO on the molecular dynamics of PVA/SSA/GO composite membranes, the complex dielectric relaxation curves were analysed.

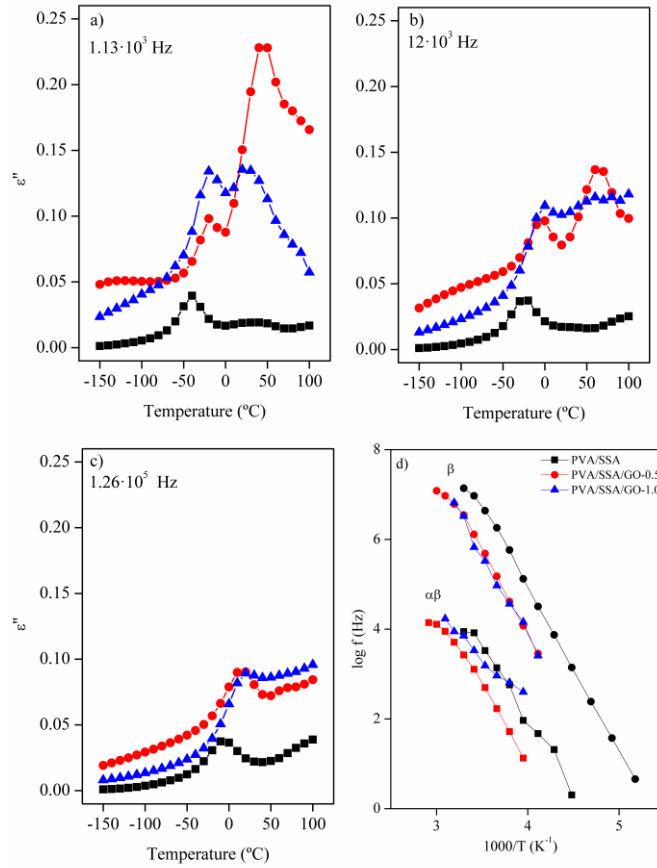


Figure 10 The imaginary part of dielectric permittivity vs temperature for the studied materials at selected frequencies and temperature dependence of the maximum relaxation time for the processes.

Loss modulus ϵ'' curves were fitted using the Havriliak-Negami (HN) model [68], [69]. In those cases, where the relaxations overlapped, the Charlesworth method was applied [70]. Dielectric curves were considered as a sum of more simple Havriliak-Negami (HN) functions (**Equation 1**).

$$\epsilon^* - \epsilon_\infty = \sum_{k=1}^{k=3} \frac{\Delta\epsilon_k}{[(1 + (i\omega\tau_{HNk})^{A_k})]^{B_k}} \quad (\text{Equation 1})$$

Where the subindex k is the number of the individual HN contributions, which can vary from $k = 1$ to 3, depending on the complexity of the ϵ'' curve at any temperature, A_k and B_k are the width and asymmetry curve parameters, $\Delta\epsilon_k$ is the dielectric strength, τ_{HNk} is the relaxation time, respectively.

To discriminate cooperative from non-cooperative segmental movements, the temperature dependence of the relaxation times with the temperature was plotted on an Arrhenius map. On the one hand, linear evolutions of $\log f$ vs T^{-1} indicate non-cooperative intramolecular segmental motions, generally associated to movements of lateral groups or movements of the main chain involving a small number of carbon atoms. On the other hand, non-linear evolutions are representative of cooperative intermolecular movements related to high-order segmental motions in the backbone. The relationship between the relaxation times and temperature for all the relaxations processes were identified as linear, which was related to an Arrhenius model [71], which corresponds to a secondary relaxation process (**Equation 2**).

$$f_{max}(T) = f_0 \cdot \exp\left(\frac{E_a}{k \cdot T}\right) \quad \text{(Equation 2)}$$

Where f_0 is the pre-exponential factor and E_a is the activation energy of the relaxation processes. The fitting parameters are summarized in **Table 3**.

Table 3. Beta and Alfa-Beta relaxation fittings to Arrhenius equation for PVA/SSA and PVA/SSA/GO composites.

Sample	Ea (kJ·mol ⁻¹)	T _{max} @ 1 kHz (°C)	R ²
PVA/SSA	69.6	-52.4	0.999
PVA/SSA/GO-0.5	71.0	-37.3	0.998
PVA/SSA/GO-1	69.5	-36.7	0.992
αβ relaxation			
PVA/SSA	61.9	-1.2	0.980
PVA/SSA/GO-0.5	65.6	18.9	0.996
PVA/SSA/GO-1	40.1	-0.4	0.983

Thus, these β and $\alpha\beta$ relaxations are attributed to local motions resulting from reorientations of polar side groups and involve small segments of the polymer of the main or lateral chain [65]–[67], [72]. The β -relaxations appear at lower temperatures and higher frequencies. This molecular origin is related to the molecular movements of the hydroxyl groups, and the water content can facilitate such movement. $\alpha\beta$ relaxations are attributed to a crankshaft type of motion of the main polymeric chain, in which a few segments are involved [65]–[67], [72]. In this case, the VFT behaviour was not observed according to DSC results. The crosslinking and the measure temperature range are the two factors that determined this behaviour. However, it should be noticed that both relaxations occurred in the range of temperatures in which the PEMFCs works. Since the molecular movement that originated them had an intramolecular origin, the protonic transport by the Grotthuss mechanism or hopping process would be favoured [73], [74]. In addition, the values obtained for the activation energy seemed to indicate that the segmental mobility of the PVA molecules decreased after the addition of GO. The shift of the peaks to higher temperatures or frequencies is mainly due to the increased relaxation time. However, according to **Table 3**, the PVA/SSA/GO-0.5 had the lowest value of E_a , indicating that this membrane would present a greater conductivity because the hopping process is favourable with decreasing the activation energy.

3.5 Electrical conductivity

Electrical conductivity is calculated from the bulk resistance, R_b , which can be determined from Ohm's Law (**Equation 3**).

$$i = R_b \cdot \Delta V \quad \text{(Equation 3)}$$

$$\sigma = \frac{l}{R_b \cdot A} \quad \text{(Equation 4)}$$

Where l is the thickness of the film, A is the electrode-electrolyte contact area and R_b is the bulk resistance of the film.

Figure 11 shows the relationship between the direct current conductivity and the frequency. In the high-frequency region, electrical conductivity increases with increasing frequency following

the universal dielectric response law. A low-frequency region, the conductivity tends to a plateau or constant value, approaching its dc value. In the intermediate region, dipolar relaxation processes are present and depend on the molecular mobility. The gradual change from plateau (dc) to a dispersive region (ac) denotes the distribution of relaxation times. The frequency dependence of electrical conductivity can be divided into distinct regions implying the existence of various dissipated effects. The polymeric chain also gains mobility of polymer segments when increasing the temperature corresponding to β and $\alpha\beta$ relaxations described above. Therefore, it favours the ionic transportation and increases the electrical conductivity. From **Figure 11** it is clear that the conductivity rises with increasing GO content.

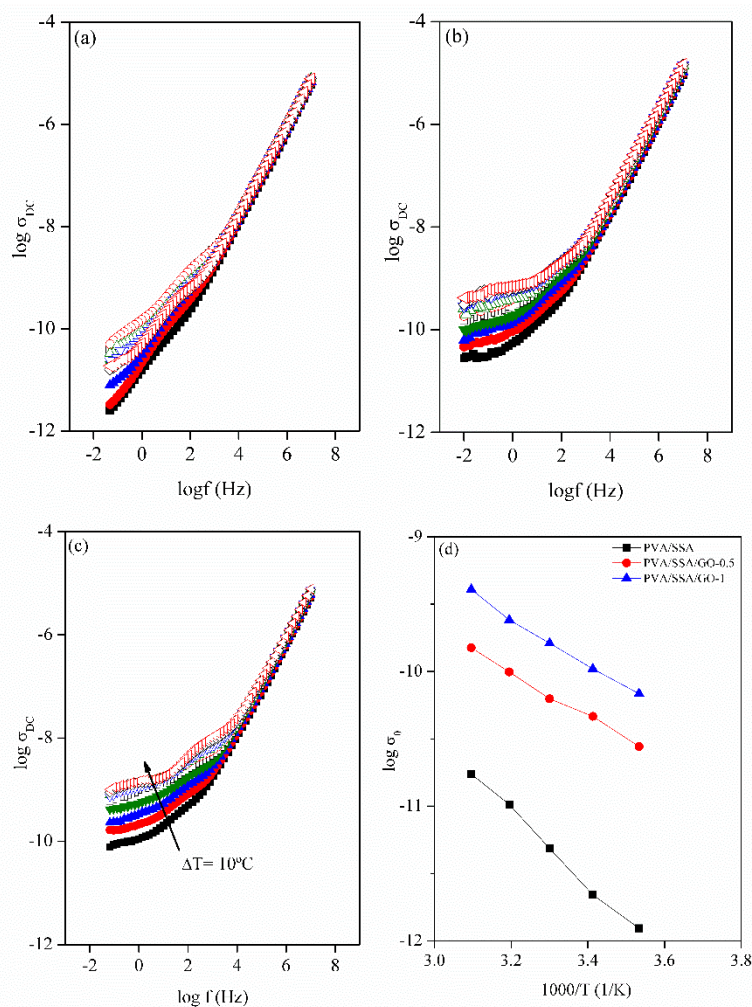


Figure 11. DC Conductivity vs f for PVA/SSA (a), 0.5 wt% composite sample (b), and 1.0 wt % composite sample (c). In panel d) DC conductivity for PVA/SSA (■), PVA/SSA/GO-0.5 (●) and PVA/SSA/GO-1.0 (▲).

Figure 11 d plots the relationship of electrical conductivity $\log \sigma_{DC}$ with the temperature that can be fitted to an Arrhenius model. If the samples could be ordered in increasing value of activation energy, it should be PVA/SSA/GO-0.5 ($31.5 \text{ kJ}\cdot\text{mol}^{-1}$), PVA/SSA/GO-1 ($33.4 \text{ kJ}\cdot\text{mol}^{-1}$), and PVA/SSA ($45.4 \text{ kJ}\cdot\text{mol}^{-1}$). As the activation energies are inversely proportional to conductivity, higher conductivity is correlated with lower activation energies. Despite the PEMFC requires low electrical conductivity, the found values are low enough, so the addition of GO does not represent a problem to use these membranes as electrolytes.

3.6 Protonic conductivity

The impedance-phase plots of the membranes at several positive temperatures are shown in **Figure 12**. Near the highest measuring frequency, 10^7 Hz, the impedance contribution is mainly due to the flow of movable ionic charges, thus the protonic conductivity can be determined from the ohmic resistance R_b of composite membranes.

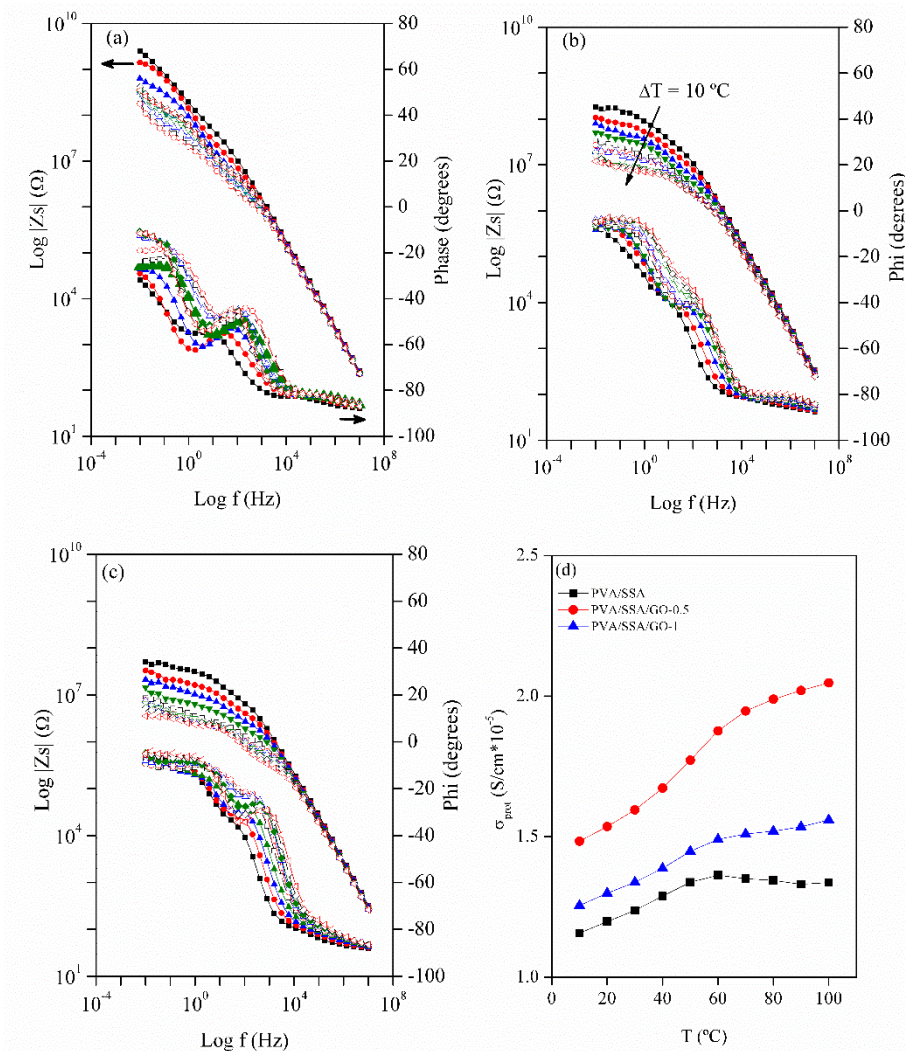


Figure 12. DC Conductivity vs f for PVA/SSA (a), 0.5 wt% composite sample (b), and 1.0 wt % composite sample (c). In panel (d) protonic conductivity evolution for PVA/SSA (■), PVA/SSA/GO-0.5 (●) and PVA/SSA/GO-1.0 (▲) with temperature.

The protonic conductivity's dependence with the temperatures for all the membranes is displayed in **Figure 12d**. It is possible to observe that the protonic conductivity increased with the temperature due to the expansion of the polymer matrix. The polymeric chain achieves faster internal vibrational modes with increasing the temperature, which weakens the interaction proton-matrix, promoting the decoupling of protons from the polymer. However, the figure shows two important characteristics since the relation of the proton conductivity with the temperature are not linear and neither increases linearly with the added GO concentration, PVA/SSA/GO-0.5 showing the higher values of them all. This tendency agrees with previous results and might be related to the existence of two dissipated effects, which can correspond to β and $\alpha\beta$ relaxations. **Figure 12d**

indicates that around 55 °C the proton conductivity significantly increased, precisely in the range of temperatures in which the PEMCF work, so their performance is significantly improved.

3.7 Polarization current and Ionic transference number

The measurement of the polarization current should give the cationic transference value when the polarization current saturates. The plot of polarized current versus time indicates that all materials start with a value of current that asymptotically tends to a lower constant value after a long time **Figure 13**. This is explained by charge carriers (ions and electrons) that move fast to the surface of the charged electrode and away from the ground electrode. It is possible to observe that the initial total current decreases with the time due to the reduction of the ionic species in the electrolyte, and becomes constant in the fully depleted situation. This is because the ionic currents through an ion-blocking electrode fall rapidly with the time when the electrolyte is primarily ionic. The charge transport in these PVA/SSA and PVA/SSA/GO composite membranes is predominantly ionic and the electronic contribution to the total current is negligible as has been calculated in **Figure 13d**. Since the matrix has carboxyl and sulfonic groups, it can act as a good proton acceptor and provide free pathways for the proton mobility.

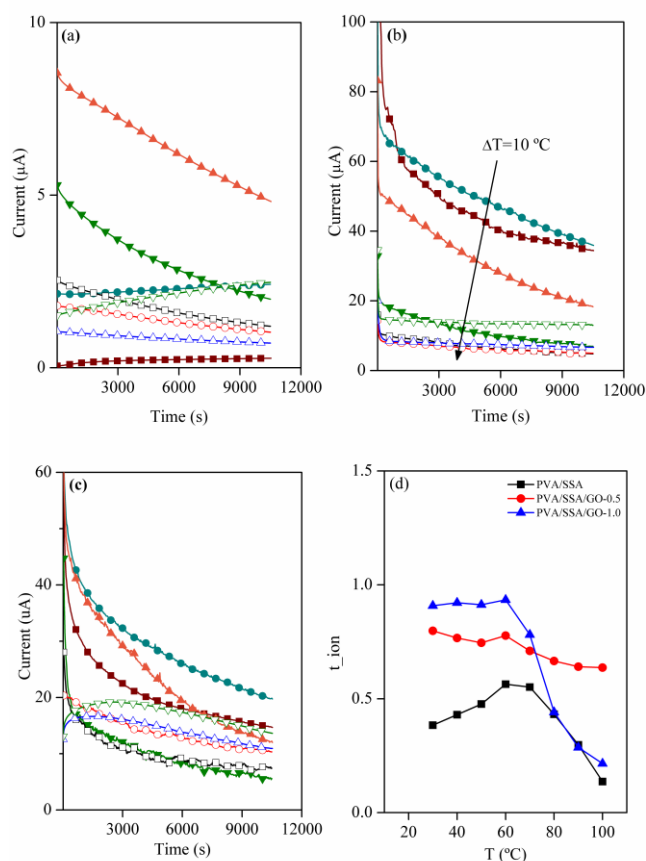


Figure 13 DC polarization current vs time plots of PVA/SSA (a), PVA/SSA/GO-0.5 (b) and PVA/SSA/GO-1.0 (c). In panel d) total ionic transference number for PVA/SSA (■), PVA/SSA/GO-0.5 (●) and PVA/SSA/GO-1.0 (▲). with temperature.

The total ionic transference number, a non-selective parameter, can then be calculated as:

$$t_{ion} = (I_0 - I_{\infty})/I_0 \quad \text{(Equation 5)}$$

with the initial (I_0) and final (I_∞) current determined from the **Equation 3**.

At room temperature, the total ionic transference numbers of PVA/SSA, and PVA/SSA/GO-0.5 PVA/SSA/GO-1.0 composite membranes are 0.464, 0.713, 0.934, respectively. It indicates that the total ionic transfer increased with the percentage of GO. Likewise, at low-temperature ionic transfer increased or stayed constant until the temperature reached around 55-60 °C. However, the total ionic transference number slightly decreased in PVA/SSA/GO-0.5 and abruptly diminished in PVA/SSA and PVA/SSA/GO-1.0 composite membranes at a singular temperature around 55-60 °C (**Figure 13d**). The effect was more intense in the composite with higher GO concentration. This indicates that the addition of GO increases the ionic nature of the membranes by adding mobile charges which could contribute positively to protonic conductivity, precisely in those temperatures in which the PEMFCs work. These results confirm that adding very low concentrations of GO to the PVA/SSA membranes can improve their electrolyte behaviour.

3.8 Measurement of single cell performance and internal resistance

The electrochemical performance of the composite membranes as fuel cell electrolyte was evaluated in a hydrogen monocell. **Figure 14** depicts the polarization curves for the fuel cells containing PVA/SSA/GO composite electrolytes. Nafion® curves are presented as reference.

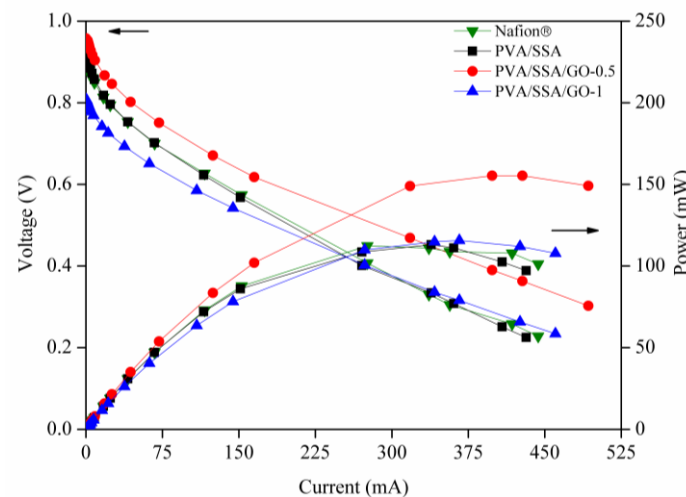


Figure 14. V vs I and P vs I curves for Nafion® and PVA/SSA/GO, 23 °C, pure hydrogen/oxygen, 2mg·cm⁻² black platinum loading, 16 cm² carbon cloth.

Power curves were fitted according to the following equation:

$$V(i) = E_0 - A \cdot \log \frac{i}{i_0} - R \cdot i \quad \text{(Equation 6)}$$

Where E_0 represents the open circuit voltage of the cell, A the Tafel slope [75], i_0 the exchange current and R the resistance of the set-up. **Table 3** collects the protonic conductivity values and the fit values of the membranes.

According to these results, the presence of GO improves fuel cell performance, most notably by introducing ionic charges and decreasing ohmic resistance. This effect seems to disappear with increasing concentration, probably due to the reduction of active surface area in the nanoparticles due to the formation of aggregates. The values obtained from the maximum values of the fuel cell

power curves are similar or better than the commercial membrane measured in the same condition, especially when the proportion of GO is low.

Table 3. Fitting parameters for the fuel cell power curves and protonic conductivity.

Sample	$\sigma_{\text{prot}} @ 30 \text{ }^{\circ}\text{C}$ ($\text{mS}\cdot\text{cm}^{-1}$)		Width (μm)	E_0 (mV)	A ($\text{mV}\cdot\text{dec}^{-1}$)	R (mOhm)	i_0 (mA)	R^2 (%)	MPP (mW)
	dry	wet							
Nafion®	3.500	17.20	112.8	915	33.0	1.15	1.12	98.4	112.32
PVA/SSA	0.012	2.06	127.9	937	39.0	1.14	1.12	99.1	113.07
PVA/SSA/GO0.5	0.016	3.06	112.0	958	45.0	0.84	2.34	97.8	155.37
PVA/SSA/GO1	0.013	1.53	142.8	808	24.8	0.96	1.37	98.7	115.72

4. Conclusions

Cross-linked PVA/SSA/GO composite membranes were prepared and a systematic characterization procedure was established to control the design of membranes for PEMFC. The addition of GO reduced the moisture content and increased thermal stability. The dielectric permittivity and the total ionic transfer number of the membranes was significantly enhanced at low filler concentration of GO. However, small agglomerates appear on the surface of membranes at concentration of 1%, which produces a reduction of these properties. In the interval of analysed temperatures, similar to PEMFC operation range, the dielectric relaxation spectrum shows β and $\alpha\beta$ relaxations processes associated to intramolecular movements, indicating that the protonic transport by the Grotthuss mechanism or hopping process might be favoured. The power produced in a hydrogen monocell when PVA/SSA/GO composite membranes act as electrolytes is similar to the commercial membrane, mainly when the proportion of GO is low. Finally, it has been proved that the systematic characterization procedure based on the study of dielectric spectra and conductivity is an adequate methodology to predict the behaviour of membranes in PEMFCs and improve their properties.

5. References

- [1] S. M. M. Ehteshami and S. H. Chan, "The role of hydrogen and fuel cells to store renewable energy in the future energy network - potentials and challenges," *Energy Policy*, vol. 73, pp. 103–109, 2014.
- [2] M. M. Mench, *Fuel cell engines*. John Wiley & Sons, 2008.
- [3] M. S. Diallo, N. A. Fromer, and M. S. Jhon, Eds., *Nanotechnology for Sustainable Development*. Springer International Publishing, 2014.
- [4] J. Rhim, C. Yeom, and S. Kim, "Modification of Poly (vinyl alcohol) Membranes Using Sulfur-succinic Acid and Its Application to Pervaporation Separation of Water -Alcohol Mixtures," *J.App.Pol.Science*, vol. 68, pp. 1717–1723, 1998.
- [5] G. Hirankumar, S. Selvasekarapandian, N. Kuwata, J. Kawamura, and T. Hattori, "Thermal, electrical and optical studies on the poly(vinyl alcohol) based polymer electrolytes," *J. Power Sources*, vol. 144, no. 1, pp. 262–267, 2005.
- [6] J. W. Rhim, H. B. Park, C. S. Lee, J. H. Jun, D. S. Kim, and Y. M. Lee, "Crosslinked poly(vinyl alcohol) membranes containing sulfonic acid group: Proton and methanol transport through membranes," *J. Memb. Sci.*, vol. 238, no. 1–2, pp. 143–151, 2004.

- [7] P. Taylor, P. B. Bhargav, B. A. Sarada, A. K. Sharma, and V. V. R. N. Rao, "Electrical Conduction and Dielectric Relaxation Phenomena of PVA Based Polymer Electrolyte Films Electrical Conduction and Dielectric Relaxation Phenomena of PVA Based Polymer Electrolyte Films," *J. Macromol. Sci. Part A Pure Appl. Chem.*, vol. 47:2, no. September 2012, pp. 131–137, 2009.
- [8] A. Awadhia, S. K. Patel, and S. L. Agrawal, "Dielectric investigations in PVA based gel electrolytes," *Prog. Cristal growth Charact. Mater.*, vol. 52, pp. 61–68, 2006.
- [9] O. G. Abdullah, S. A. Hussien, and A. Alani, "Electrical Characterization of Polyvinyl Alcohol Films Doped with Sodium Iodide," *Asian Trans. Sci. Technol.*, vol. 1, no. 4, pp. 1–4, 2011.
- [10] T. A. Hanafy, "Dielectric relaxation and alternating current conductivity of lanthanum , gadolinium , and erbium-polyvinyl alcohol doped films Dielectric relaxation and alternating current conductivity of lanthanum , gadolinium , and erbium-polyvinyl alcohol doped films," *J. Appl. Phys.*, vol. 34102, no. 112, 2012.
- [11] A. Fattoum, M. Arous, R. Pedicini, A. Carbone, and C. Charnay, "Conductivity and Dielectric Relaxation in Crosslinked PVA by Oxalic and Citric Acids," *Polym. Sci.*, vol. 57, no. 3, pp. 321–329, 2015.
- [12] A. Fattoum and M. Arous, "Conductivity and Dielectric Relaxation in Various Polyvinyl Alcohol / Ammonium Salt Composites," *Polym. Sci.*, vol. 56, no. 6, pp. 907–916, 2014.
- [13] C. V. S. Reddy, A. K. Sharma, and V. V. R. N. Rao, "Conductivity and discharge characteristics of polyblend (PVP+PVA+KIO 3) electrolyte," *J. Power Sources*, vol. 114, pp. 338–345, 2003.
- [14] R. J. Sengwa and S. Choudhary, "Investigation of correlation between dielectric parameters and nanostructures in aqueous solution grown poly (vinyl alcohol) - montmorillonite clay nanocomposites by dielectric," *eXPRESS Polym. Lett.*, vol. 4, no. 9, pp. 559–569, 2010.
- [15] A. Nigrawal and N. Chand, "Electrical and Dynamic Mechanical Analysis of Nano Alumina Addition on Polyvinyl Alcohol (PVA) Composites," *Prog. Nanotechnol. Nanomater.*, vol. 2, pp. 25–33, 2013.
- [16] Y.-L. L. Suryani , Yu-Nan Chang, Juin-Yih Lai, "PBI functionalized silica nanoparticles," *J Memb Sci*, vol. 1, no. 7, pp. 403–404, 2012.
- [17] P. Jannasch, "Recent developments in high-temperature proton conducting polymer electrolyte membranes," *Curr. Opin. Colloid Interface Sci.*, no. 8, pp. 96–102, 2003.
- [18] B. J. Liang, Y. Huang, L. Zhang, Y. Wang, Y. Ma, T. Guo, and Y. Chen, "Molecular-Level Dispersion of Graphene into Poly (vinyl alcohol) and Effective Reinforcement of their Nanocomposites," *Adv.Funct.Mater*, vol. 19, pp. 2297–2302, 2009.
- [19] M. J. Mcallister, J. Li, D. H. Adamson, H. C. Schniepp, A. a Abdala, J. Liu, O. M. Herrera-alonso, D. L. Milius, R. Car, R. K. Prud, and I. a Aksay, "Expansion of Graphite," *Society*, vol. 19, no. 4, pp. 4396–4404, 2007.
- [20] J. Song, X. Wang, and C. Chang, "Preparation and Characterization of Graphene Oxide," *J nanomat.*, vol. 2014, 2014.
- [21] D. Cai and M. Song, "Recent advance in functionalized graphene/polymer nanocomposites," *J. Mater. Chem.*, vol. 20, no. 37, p. 7906, 2010.

- [22] S. Niyogi, E. Bekyarova, M. E. Itkis, J. L. McWilliams, M. a Hamon, and R. C. Haddon, "Solution properties of graphite and graphene.," *J. Am. Chem. Soc.*, vol. 128, no. 24, pp. 7720–1, 2006.
- [23] S. Ghosh, R. Ghosh, P. Kumar Guha, and T. K. Bhattacharyya, "Enhanced proton conductivity of graphene oxide/nafion composite material in humidity sensing application," *IEEE Trans. Nanotechnol.*, vol. 15, no. 5, pp. 782–790, 2016.
- [24] M. R. Karim, K. Hatakeyama, T. Matsui, H. Takehira, T. Taniguchi, M. Koinuma, Y. Matsumoto, T. Akutagawa, T. Nakamura, S. I. Noro, T. Yamada, H. Kitagawa, and S. Hayami, "Graphene oxide nanosheet with high proton conductivity," *J. Am. Chem. Soc.*, vol. 135, no. 22, pp. 8097–8100, 2013.
- [25] R. B. E. and W. G. McCrum N. G., *Anelastic and dielectric effects in polymeric solids*, Dover ed. 1991.
- [26] B. Schartel, J. Wendling, and J. H. Wendorff, "Cellulose/Poly(vinyl alcohol) Blends. 1. Influence of Miscibility and Water Content on Relaxations," *Macromolecules*, vol. 29, no. 5, pp. 1521–1527, 1996.
- [27] A. De La Rosa, L. Heux, and J. Y. Cavaille, "Secondary relaxations in poly(allyl alcohol), PAA, and poly(vinyl alcohol), PVA. II. Dielectric relaxations compared with dielectric behaviour of amorphous dried and hydrated cellulose and dextran," *Polymer (Guildf.)*, vol. 42, no. 12, pp. 5371–5379, 2001.
- [28] N. Ni and K. Zhao, "Dielectric analysis of chitosan gel beads suspensions: Influence of low crosslinking agent concentration on the dielectric behavior," *J. Colloid Interface Sci.*, vol. 312, no. 2, pp. 256–264, 2007.
- [29] K. P. Singh and P. N. Gupta, "Study of of dielectric relaxation in polymer electrolytes," *Eur. Polym.*, vol. 34, no. 7, pp. 1023–1029, 1998.
- [30] F. H. Abd El-kader, W. H. Osman, K. H. Mahmoud, and M. A. F. Basha, "Dielectric investigations and ac conductivity of polyvinyl alcohol films doped with europium and terbium chloride," *Phys. B Condens. Matter*, vol. 403, no. 19–20, pp. 3473–3484, 2008.
- [31] R. Mishra and K. J. Rao, "Electrical conductivity studies of poly(ethyleneoxide)-poly(vinylalcohol) blends," *Solid State Ionics*, vol. 106, no. 1–2, pp. 113–127, 1998.
- [32] P. Dutta, S. Biswas, and S. K. De, "Dielectric relaxation in polyaniline-polyvinyl alcohol composites," *Mater. Res. Bull.*, vol. 37, pp. 193–200, 2002.
- [33] B. C. Shekar, V. Veeravazhuthi, S. Sakthivel, D. Mangalaraj, and S. K. Narayandass, "Growth , structure , dielectric and AC conduction properties of solution grown PVA ® lms," *Thin Solid Films*, vol. 348, pp. 122–129, 1999.
- [34] R. J. Sengwa and S. Sankhla, "Dielectric dispersion study of coexisting phases of aqueous polymeric solution: Poly(vinyl alcohol) + poly(vinyl pyrrolidone) two-phase systems," *Polymer (Guildf.)*, vol. 48, no. 9, pp. 2737–2744, 2007.
- [35] I. Tantis, G. C. Psarras, and D. Tasis, "Functionalized graphene – poly (vinyl alcohol) nanocomposites : Physical and dielectric properties," *eXPRESS Polym. Lett.*, vol. 6, no. 4, pp. 283–292, 2012.
- [36] W. S. Hummers and R. E. Offeman, "Preparation of Graphitic Oxide," *J. Am. Chem. Soc.*, vol. 80, no. 6, pp. 1339–1339, 1958.
- [37] L. Shahriary and A. A. Athawale, "Graphene Oxide Synthesized by using Modified

- Hummers Approach,” *Int. J. Renew. Energy Environ. Eng.*, vol. 2, no. 1, 2014.
- [38] A. R.-G. A. Martinez-Felipe, C. Moliner-Estopinan, C. T. Imrie, “Characterization of Crosslinked Poly(vinyl alcohol)-Based Membranes with Different Hydrolysis Degrees for Their Use as Electrolytes in Direct Methanol Fuel Cells,” *Polym. Polym. Compos.*, vol. 124, pp. 1000–1011, 2012.
- [39] T. A. Zawodzinski, “Water Uptake by and Transport Through Nafion® 117 Membranes,” *J. Electrochem. Soc.*, vol. 140, no. 4, p. 1041, 1993.
- [40] D. G. Papageorgiou, I. A. Kinloch, and R. J. Young, “Mechanical Properties of Graphene and Graphene-based Nanocomposites,” *Prog. Mater. Sci.*, vol. 90, no. July, pp. 75–127, 2017.
- [41] L. Duan, R. Hao, Z. Xu, X. He, A. S. Adeleye, and Y. Li, “Removal of graphene oxide nanomaterials from aqueous media via coagulation: Effects of water chemistry and natural organic matter,” *Chemosphere*, vol. 168, pp. 1051–1057, 2017.
- [42] Y. Zou, X. Wang, Y. Ai, Y. Liu, J. Li, Y. Ji, and X. Wang, “Coagulation Behavior of Graphene Oxide on Nanocrystalline Mg/Al Layered Double Hydroxides: Batch Experimental and Theoretical Calculation Study,” *Environ. Sci. Technol.*, vol. 50, no. 7, pp. 3658–3667, 2016.
- [43] K.-J. Kim, S.-B. Lee, and N. W. Han, “Effects of the Degree of Crosslinking on Properties of Poly(vinyl alcohol) Membranes,” *Polymer Journal*, vol. 25, no. 12. pp. 1295–1302, 1993.
- [44] S. Xiao, R. Y. M. Huang, and X. Feng, “Preparation and properties of trimesoyl chloride crosslinked poly(vinyl alcohol) membranes for pervaporation dehydration of isopropanol,” *J. Memb. Sci.*, vol. 286, no. 1–2, pp. 245–254, 2006.
- [45] L. K. Pandey, C. Saxena, and V. Dubey, “Modification of poly(vinyl alcohol) membranes for pervaporative separation of benzene/cyclohexane mixtures,” *J. Memb. Sci.*, vol. 227, no. 1–2, pp. 173–182, 2003.
- [46] J. M. Gohil, A. Bhattacharya, and P. Ray, “Studies on the cross-linking of poly (vinyl alcohol),” *J. Polym. Res.*, vol. 13, no. 2, pp. 161–169, 2006.
- [47] A. M. Shehap, “Thermal and Spectroscopic Studies of Polyvinyl Alcohol/Sodium Carboxy Methyl Cellulose Blends,” *Egypt. J. Solids*, vol. 31, no. 31, pp. 75–91, 2008.
- [48] H. S. Mansur, C. M. Sadahira, A. N. Souza, and A. A. P. Mansur, “FTIR spectroscopy characterization of poly (vinyl alcohol) hydrogel with different hydrolysis degree and chemically crosslinked with glutaraldehyde,” *Mater. Sci. Eng. C*, vol. 28, no. 4, pp. 539–548, 2008.
- [49] J. Ding, C. Chuy, and S. Holdcroft, “A self-organized network of nanochannels enhances ion conductivity through polymer films,” *Chem. Mater.*, vol. 13, no. 7, pp. 2231–2233, 2001.
- [50] K. Pourzare, Y. Mansourpanah, and S. Farhadi, “Advanced nanocomposite membranes for fuel cell applications: a comprehensive review,” *Biofuel Res. J.*, vol. 3, no. 4, pp. 496–513, 2016.
- [51] G. Socrates, *Infrared and Raman Characteristic Groups Frequencies*. 2004.
- [52] P. R. B. Kalim Deshmukh, M. Basheer Ahamed, S.K. Khadheer Pasha, Rajendra R. Deshmukh, “Highly Dispersible Graphene Oxide Reinforced Polypyrrole/Polyvinyl

- alcohol Blend Nanocomposites with High Dielectric Constant and Low Dielectric Loss Kalim,” *RSC Adv.* 5, pp. 61933–61945, 2015.
- [53] S. K. K. Pasha, K. Deshmukh, M. B. Ahamed, K. Chidambaram, M. K. Mohanapriya, and N. A. N. Raj, “Investigation of Microstructure, Morphology, Mechanical, and Dielectric Properties of PVA/PbO Nanocomposites,” *Adv. Polym. Technol.*, vol. 36, no. January 2016, p. n/a-n/a, 2015.
- [54] H. Beydaghi, M. Javanbakht, and E. Kowsari, “Synthesis and characterization of poly(vinyl alcohol)/Sulfonated graphene oxide nanocomposite membranes for use in proton exchange membrane fuel cells (PEMFCs),” *Ind. Eng. Chem. Res.*, vol. 53, no. 43, pp. 16621–16632, 2014.
- [55] S. Khilari, S. Pandit, M. M. Ghangrekar, D. Pradhan, and D. Das, “Graphene oxide-impregnated PVA-STA composite polymer electrolyte membrane separator for power generation in a single-chambered microbial fuel cell,” *Ind. Eng. Chem. Res.*, vol. 52, no. 33, pp. 11597–11606, 2013.
- [56] O. García-Valdez, R. Ledezma-Rodríguez, E. Saldívar-Guerra, L. Yate, S. Moya, and R. F. Ziolo, “Graphene oxide modification with graft polymers via nitroxide mediated radical polymerization,” *Polym. (United Kingdom)*, vol. 55, no. 10, pp. 2347–2355, 2014.
- [57] C. Bao, Y. Guo, L. Song, and Y. Hu, “Poly(vinyl alcohol) nanocomposites based on graphene and graphite oxide: a comparative investigation of property and mechanism,” *J. Mater. Chem.*, vol. 21, no. 36, p. 13942, 2011.
- [58] G. Gonçalves, P. A. A. P. Marques, A. Barros-Timmons, I. Bdkin, M. K. Singh, N. Emami, and J. Grácio, “Graphene oxide modified with PMMA via ATRP as a reinforcement filler,” *J. Mater. Chem.*, vol. 20, no. 44, p. 9927, 2010.
- [59] S. Morimune, T. Nishino, and T. Goto, “Poly(vinyl alcohol)/graphene oxide nanocomposites prepared by a simple eco-process,” *Polym. J.*, vol. 44, no. 10, pp. 1056–1063, 2012.
- [60] H. J. Salavagione, G. Martínez, and M. A. Gómez, “Synthesis of poly(vinyl alcohol)/reduced graphite oxide nanocomposites with improved thermal and electrical properties,” *J. Mater. Chem.*, vol. 19, no. 28, p. 5027, 2009.
- [61] J. M. Morancho, J. M. Salla, A. Cadenato, X. Fernández-Francos, X. Ramis, P. Colomer, Y. Calventus, and R. Ruíz, “Kinetic studies of the degradation of poly(vinyl alcohol)-based proton-conducting membranes at low temperatures,” *Thermochim. Acta*, vol. 521, no. 1–2, pp. 139–147, 2011.
- [62] C.-Y. Tseng, Y.-S. Ye, K.-Y. Kao, J. Joseph, W.-C. Shen, J. Rick, and B.-J. Hwang, “Interpenetrating network-forming sulfonated poly(vinyl alcohol) proton exchange membranes for direct methanol fuel cell applications,” *Int. J. Hydrogen Energy*, vol. 36, no. 18, pp. 11936–11945, 2011.
- [63] X. Yang, L. Li, S. Shang, and X. Tao, “Synthesis and characterization of layer-aligned poly(vinyl alcohol)/graphene nanocomposites,” *Polymer (Guildf.)*, vol. 51, no. 15, pp. 3431–3435, 2010.
- [64] S. Yun, H. Im, Y. Heo, and J. Kim, “Crosslinked sulfonated poly(vinyl alcohol)/sulfonated multi-walled carbon nanotubes nanocomposite membranes for direct methanol fuel cells,” *J. Memb. Sci.*, vol. 380, no. 1–2, pp. 208–215, 2011.
- [65] N. N. Rozik and A. A. Ward, “A novel approach on poly(ionic liquid)-based poly(vinyl

- alcohol) as a hydrophilic/hydrophobic conductive polymer electrolytes,” *Polym. Bull.*, 2017.
- [66] A. S. Hickey and N. A. Peppas, “Mesh size and diffusive characteristics of semicrystalline poly(vinyl alcohol) membranes prepared by freezing/thawing techniques,” *J. Memb. Sci.*, vol. 107, no. 3, pp. 229–237, 1995.
- [67] J. B. Gonzalez-Campos, E. Prokhorov, I. C. Sanchez, J. G. Luna-Barcenas, A. Manzano-Ramirez, J. Gonzalez-Hernandez, Y. Lopez-Castro, and R. E. Del Rio, “Molecular dynamics analysis of PVA-AgnP composites by dielectric spectroscopy,” *J. Nanomater.*, vol. 2012, 2012.
- [68] S. Havriliak and S. Negami, “A complex plane representation of dielectric and mechanical relaxation processes in some polymers,” *Polymer (Guildf)*, vol. 8, pp. 161–210, 1967.
- [69] S. Havriliak and S. Negami, “A complex plane analysis of α -dispersions in some polymer systems,” *J. Polym. Sci. Part C Polym. Symp.*, vol. 14, no. 1, pp. 99–117, Mar. 1966.
- [70] J. M. Charlesworth, “Deconvolution of overlapping relaxations in dynamic mechanical spectra,” *J. Mater. Sci.*, vol. 28, no. 2, pp. 399–404, 1993.
- [71] J. D. Ferry, *Viscoelastic properties of polymers*. John Wiley & Sons, 1980.
- [72] S. L. A.-E.-M. A.S. El-Houssiny, A.A. M. Ward, S.H. Mansour, “Biodegradable Blends Based on Polyvinyl Pyrrolidone for insulation Purposes,” *J. Appl. Polym. Sci.*, vol. 124, pp. 3879–3891, 2012.
- [73] C. Gainaru, E. W. Stacy, V. Bocharova, M. Gobet, A. P. Holt, T. Saito, S. Greenbaum, and A. P. Sokolov, “Mechanism of Conductivity Relaxation in Liquid and Polymeric Electrolytes: Direct Link between Conductivity and Diffusivity,” *J. Phys. Chem. B*, vol. 120, no. 42, pp. 11074–11083, 2016.
- [74] D. P. Almond and A. R. West, “Mobile ion concentrations in solid electrolytes from an analysis of a.c. conductivity,” *Solid State Ionics*, vol. 9–10, no. PART 1, pp. 277–282, 1983.
- [75] J. Tafel, “Über die Polarisation bei kathodischer Wasserstoffentwicklung,” *Zeit. Phys. Chem*, vol. 50A, p. 641, 1905.

Acknowledgements

The authors would like to thank Dr. Roberto Teruel Juanes and Dr. Victor Saenz de Juano for their advice in the treatment of results. The authors are also thankful to Generalitat Valenciana for the Santiago Grisolia scholarship, GRISOLIA/2013/03, the European Regional Development Funds and the Spanish Ministry of Science and Innovation for the concession of Research Projects ENE2014-53734-C2-1-R

ANNEX – OPEN ACCESS POLICIES

... opening access to research
Home • Search • Journals • Publishers • FAQ • Suggest • About

Search - Publisher copyright policies & self-archiving

[English](#) | [Español](#) | [Magyar](#) | [Nederlands](#) | [Português](#)

One journal found when searched for: **polymer testing**

Journal:	Polymer Testing (ISSN: 0142-9418; EISSN: 1873-2348)
RoMEO:	This is a RoMEO green journal
Paid OA:	A paid open access option is available for this journal.
Author's Pre-print:	✓ author can archive pre-print (ie pre-refereeing)
Author's Post-print:	✓ author can archive post-print (ie final draft post-refereeing)
Publisher's Version/PDF:	✗ author cannot archive publisher's version/PDF
General Conditions:	<ul style="list-style-type: none">• Authors pre-print on any website, including arXiv and RePEc• Author's post-print on author's personal website immediately• Author's post-print on open access repository after an embargo period of between 12 months and 48 months• Permitted deposit due to Funding Body, Institutional and Governmental policy or mandate, may be required to comply with embargo periods of 12 months to 48 months• Author's post-print may be used to update arXiv and RePEc• Publisher's version/PDF cannot be used• Must link to publisher version with DOI• Author's post-print must be released with a Creative Commons Attribution Non-Commercial No Derivatives License
Mandated OA:	(Awaiting information)
Paid Open Access:	Open Access
Notes:	<ul style="list-style-type: none">• Publisher last reviewed on 03/09/2015
Copyright:	Unrashing the power of academic sharing - Sharing Policy - Sharing and Hosting Policy FAQ - Green open access - Journal Embargo Period List (pdf) - Journal Embargo List for UK Authors - Attaching a User License (pdf) - Funding Body Agreements
Updated:	01-May-2015 - Suggest an update for this record
Link to this page:	http://www.sherpa.ac.uk/romeo/list.do?id=142-9418
Published by:	Elsevier - Green Policies in RoMEO

This summary is for the journal's default policies, and changes or exceptions can often be negotiated by authors.
All information is correct to the best of our knowledge but should not be relied upon for legal advice.